AIAA Aviation Forum and ASCEND co-located Conference Proceedings
21 - 25 July 2025, Las Vegas, Nevada
AIAA AVIATION FORUM AND ASCEND 2025

10.2514/6.2025-3280

Time-Domain Boundary Integral Equation for moving acoustic sources in uniform flow and its solution by an advanced time propagation approach

Fang Q. Hu*
Old Dominion University, Norfolk, VA 23529, USA

Douglas M. Nark†
NASA Langley Research Center, Hampton, VA 23681-2199, USA

This paper presents a time-domain boundary integral equation (TDBIE) formulation for predicting acoustic scattering from moving sources in a uniform mean flow. This work is motivated by the increasing need for accurate aeroacoustic modeling of modern aircraft configurations, including VTOL and eVTOL systems with rotating components. A key challenge in time-domain scattering simulations with moving sources is the determination of retarded time for a given observer time, which involves solving an implicit equation at each time step. This can be computationally costly, particularly for numerical solution of the TDBIE where every surface element on the scattering body acts as an observer. To address this, a Non-uniform Grid Interpolation Distribution Algorithm (NGIDA), which is a high-order accurate algorithm that avoids the need for solving retarded-time equations, is introduced. The high-order accuracy is beneficial for resolving acoustic waves at high frequencies. The method converts interpolation-based values from a non-uniform advanced time grid onto a uniformly spaced observer time grid. It achieves high-order accuracy while avoiding repeated evaluations of the acoustic signal, thereby significantly reducing memory requirements and computational cost. Numerical examples involving both rotational and rectilinear source motions are presented for validation. Scattering by rigid and lined flat plates is simulated, and results are shown to agree closely with analytical solutions, demonstrating the accuracy and efficiency of the proposed approach.

I. Introduction

Accurately predicting acoustic scattering and shielding from moving sources is increasingly important in aeroacoustic applications, particularly for VTOL and eVTOL aircraft with rotating components such as propellers and rotors. As these aircraft become more popular, managing their acoustic footprint is essential to reducing noise pollution and meeting regulatory standards in urban environments. Time-domain simulation methods are especially well-suited for predicting sound propagation and scattering from moving acoustic sources, providing notable advantages over frequency-domain approaches. Unlike frequency-domain methods, time-domain simulations can capture transient and non-periodic acoustic fields associated with moving sources, making them effective for modeling complex, unsteady noise environments. This capability offers a distinct advantage in designing noise mitigation strategies for advanced aircraft configurations.

This paper presents a formulation of the Time-Domain Boundary Integral Equation (TDBIE) for the scattering of acoustic fields generated by sources in motion within a uniform mean flow. While the time-domain boundary element method follows a similar solution procedure as for stationary sources, determining the retarded time corresponding to a given observer time requires solving an implicit algebraic equation at each time step for every observer location. This process can be computationally expensive when solving the TDBIE where every surface element on the scattering body acts as an observer.

It has long been recognized that the implicit solution for retarded time can be avoided by using an advanced time propagation approach to compute the acoustic field generated by moving sources[1–6]. A key challenge in implementing

*Professor, Department of Mathematics and Statistics, AIAA Associate Fellow
†Senior Research Scientist, Applied Acoustics Branch, Research Directorate, AIAA Associate Fellow

such a model arises from the fact that the observer times corresponding to uniformly spaced source times are generally non-uniform when the sources are in motion. As a result, interpolation is typically required to evaluate the acoustic field at the desired uniformly spaced observer time grid. For instance, linear and spline interpolations were used in Ref. [1], while a "source-time-dominant" algorithm was proposed in Ref. [4]. The latter was found to require significantly fewer operations in maneuvering rotor noise predictions[5]. More recently, Ref. [3] presented an advanced time approach for acoustic analogy predictions, wherein the acoustic signal was progressively constructed using a linear interpolation strategy.

In this paper, we present a systematic advanced time propagation approach based on high-order interpolation polynomials. As in previous work, the acoustic signal is progressively built. However, our high-order accurate algorithm converts interpolation-based evaluations from a non-uniform advanced time grid onto a uniformly spaced observer time grid via a distribution process. We refer to this method as the Non-uniform Grid Interpolation Distribution Algorithm (NGIDA). The NGIDA eliminates the need for repeated evaluations of the acoustic signal that are often required in existing methods when high-order interpolation is employed. It is formulated using high-order interpolation techniques to ensure numerical accuracy, particularly in capturing high-frequency acoustic content[7].

Numerical examples are provided to validate the proposed formulation. These include scattering of acoustic fields generated by sources in both rotational and rectilinear motion, interacting with rigid and lined plates. Comparisons with analytical solutions are also presented.

The rest of the paper is organized as follows. In Section II, the TDBIE for the scattering of acoustic sources in motion within a uniform mean flow is formulated. The NGIDA method is presented in Section III and numerical examples are given in Section IV. Section V has the concluding remarks.

II. Formulation of Time-Domain Boundary Integral Equation with sources in motion

In this section, we provide essential steps in deriving the time domain boundary integral equation for scattering of acoustic sources in motion in a constant mean flow. We start with the convective wave equation that has a source term:

$$\left(\frac{\partial}{\partial t} + \boldsymbol{U}\cdot\nabla\right)^2 p - c^2\nabla^2 p = s(\boldsymbol{r},t) \tag{1}$$

and homogeneous initial conditions:

$$p(\boldsymbol{r},0) = \frac{\partial p}{\partial t}(\boldsymbol{r},0) = 0, \quad t = 0. \tag{2}$$

In the above, c is the speed of sound, $\boldsymbol{U}$ is the constant mean velocity, and $s(\boldsymbol{r},t)$ represents the known acoustic source. Furthermore, in addition to the radiation condition at the far field, Eqs. (1) and (2) are to be supplemented with boundary conditions on a scattering surface S.

The convective wave equation (Eq. 1) and the initial condition (Eq. 2) as well as the boundary conditions can be reformulated into an integral equation. To facilitate the conversion, following Ref. [8], introduce a free-space Green's function $\tilde{G}(\boldsymbol{r},t;\boldsymbol{r}',t')$ that is defined as follows:

$$\left(\frac{\partial}{\partial t} + \boldsymbol{U}\cdot\nabla\right)^2 \tilde{G} - c^2\nabla^2\tilde{G} = \delta(\boldsymbol{r}-\boldsymbol{r}')\delta(t-t') \tag{3}$$

with the following causality conditions

$$\tilde{G}(\boldsymbol{r},t;\boldsymbol{r}',t') = \frac{\partial\tilde{G}}{\partial t}(\boldsymbol{r},t;\boldsymbol{r}',t') = 0, \quad t > t'. \tag{4}$$

The solution to Eqs. (3) and (4) is well-known (see, e.g., [8–10]):

$$\tilde{G}(\boldsymbol{r},t;\boldsymbol{r}',t') = \frac{G_0}{4\pi c^2}\delta\left(t'-t+\boldsymbol{\beta}\cdot(\boldsymbol{r}'-\boldsymbol{r}) - \frac{\bar{R}(\boldsymbol{r}',\boldsymbol{r})}{c\alpha^2}\right) \tag{5}$$

where

$$G_0 = \frac{1}{\bar{R}(\boldsymbol{r}', \boldsymbol{r})}, \quad \text{and} \quad \bar{R}(\boldsymbol{r}', \boldsymbol{r}) = \sqrt{[\boldsymbol{M} \cdot (\boldsymbol{r}' - \boldsymbol{r})]^2 + \alpha^2 |\boldsymbol{r}' - \boldsymbol{r}|^2} \tag{6}$$

in which

$$\boldsymbol{M} = \frac{\boldsymbol{U}}{c}, \quad \alpha = \sqrt{1 - M^2}, \quad \boldsymbol{\beta} = \frac{\boldsymbol{U}}{c^2 - U^2} = \frac{\boldsymbol{U}}{c^2 \alpha^2} = \frac{\boldsymbol{M}}{c\alpha^2}, \quad U = |\boldsymbol{U}|, \quad M = |\boldsymbol{M}|. \tag{7}$$

For convenience of discussion, as in Ref. [8], define a *modified normal derivative* (denoted by an overbar) as

$$\frac{\partial}{\partial \bar{n}} = \frac{\partial}{\partial n} - M_n (\boldsymbol{M} \cdot \nabla) \tag{8}$$

and a *combined normal derivative* (denoted by a tilde) as

$$\frac{\partial}{\partial \tilde{n}} = \frac{\partial}{\partial n} - \frac{M_n}{c} \left(\frac{\partial}{\partial t} + \boldsymbol{U} \cdot \nabla \right) = \frac{\partial}{\partial \bar{n}} - \frac{M_n}{c} \frac{\partial}{\partial t} \tag{9}$$

where $M_n = \boldsymbol{M} \cdot \boldsymbol{n}$ and $\boldsymbol{n}$ denotes the unit normal vector (in the direction out of the fluid domain) on the scattering surface S. Then, utilizing the Green's function $\tilde{G}(\boldsymbol{r}, t; \boldsymbol{r}', t')$, Eq. (1) can be converted into an integral relation of the following form:

$$p(\boldsymbol{r}', t') = Q(\boldsymbol{r}', t') + \frac{1}{4\pi} \int_S \left[G_0 \frac{\partial p}{\partial \tilde{n}}(\boldsymbol{r}_s, t'_R) - \frac{\partial G_0}{\partial \bar{n}} \left(p(\boldsymbol{r}_s, t'_R) + \frac{\bar{R}}{c\alpha^2} \frac{\partial p}{\partial t}(\boldsymbol{r}_s, t'_R) \right) \right] d\boldsymbol{r}_s \tag{10}$$

where $\boldsymbol{r}_s$ denotes points on the scattering surface S. Here, $\boldsymbol{r}'$ and t' denote, respectively, the observer point and time off the scattering surface S. Also, t'_R in Eq. (10) is the retarded time with respect to observer $\boldsymbol{r}'$ and t' and is defined as

$$t'_R = t' + \boldsymbol{\beta} \cdot (\boldsymbol{r}' - \boldsymbol{r}_s) - \frac{\bar{R}(\boldsymbol{r}', \boldsymbol{r}_s)}{c\alpha^2}. \tag{11}$$

The integral relation, Eq. (10), yields a Time Domain Boundary Integral Equation (TDBIE) by taking the limit $\boldsymbol{r}' \to \boldsymbol{r}'_s$ where $\boldsymbol{r}'_s$ is a point on the surface of the scattering body[8]:

$$\frac{1}{2} p(\boldsymbol{r}'_s, t') = Q(\boldsymbol{r}_s{}', t') + \frac{1}{4\pi} \int_S \left[G_0 \frac{\partial p}{\partial \tilde{n}}(\boldsymbol{r}_s, t'_R) - \frac{\partial G_0}{\partial \bar{n}} \left(p(\boldsymbol{r}_s, t'_R) + \frac{\bar{R}}{c\alpha^2} \frac{\partial p}{\partial t}(\boldsymbol{r}_s, t'_R) \right) \right] d\boldsymbol{r}_s \tag{12}$$

Solving Eq. (12) gives the surface pressure when the boundary condition for $\partial p / \partial \tilde{n}$ is known. Then, Eq. (10) can be used to predict the pressure at any observer point off the scattering body.

We note that $Q(\boldsymbol{r}', t')$ in Eq. (10) denotes the contribution at observer point $\boldsymbol{r}'$ and observer time t' by the source term $s(\boldsymbol{r}, t)$:

$$Q(\boldsymbol{r}', t') = \int_{-\infty}^{\infty} \int_V \tilde{G}(\boldsymbol{r}, t; \boldsymbol{r}', t') s(\boldsymbol{r}, t) d\boldsymbol{r} dt$$

in which V is the region enclosing acoustic sources.

Now consider the case of a point source in motion. Specifically, assume

$$s(\boldsymbol{r}, t) = q(t) \delta(\boldsymbol{r} - \boldsymbol{r}_q(t)) \tag{13}$$

where $\boldsymbol{r}_q(t)$ denotes the location of a moving source point as a function of time t. Then, the contribution by the source term becomes the following:

$$Q(\boldsymbol{r}', t) = \int_{-\infty}^{\infty} \int_{V_s} \tilde{G}(\boldsymbol{r}, t; \boldsymbol{r}', t') q(t) \delta(\boldsymbol{r} - \boldsymbol{r}_q(t)) d\boldsymbol{r} dt$$

$$= \int_{-\infty}^{\infty} \int_{V_s} \frac{1}{4\pi c^2 \bar{R}(\boldsymbol{r}', \boldsymbol{r})} \delta \left(t' - t + \boldsymbol{\beta} \cdot (\boldsymbol{r}' - \boldsymbol{r}) - \frac{\bar{R}(\boldsymbol{r}', \boldsymbol{r})}{c\alpha^2} \right) q(t) \delta(\boldsymbol{r} - \boldsymbol{r}_q(t)) d\boldsymbol{r} dt$$

$$= \int_{-\infty}^{\infty} \frac{1}{4\pi c^2 \bar{R}(\boldsymbol{r}', \boldsymbol{r}_q(t))} \delta\left(t' - t + \boldsymbol{\beta} \cdot (\boldsymbol{r}' - \boldsymbol{r}_q(t)) - \frac{\bar{R}(\boldsymbol{r}', \boldsymbol{r}_q(t))}{c\alpha^2}\right) q(t) dt. \tag{14}$$

To simplify the integral, introduce

$$g(t) = t' - t + \boldsymbol{\beta} \cdot (\boldsymbol{r}' - \boldsymbol{r}_q(t)) - \frac{\bar{R}(\boldsymbol{r}', \boldsymbol{r}_q(t))}{c\alpha^2}. \tag{15}$$

where we have [11]

$$\delta(g(t)) = \sum_i \frac{\delta(t - t_i)}{|dg/dt|}$$

in which t_i denotes the zeros of $g(t)$, i.e., $g(t_i) = 0$. In this paper, we assume the source motion is subsonic and $g(t) = 0$ has only a unique solution. Let t_e be the root of

$$g(t_e) = t' - t_e + \boldsymbol{\beta} \cdot (\boldsymbol{r}' - \boldsymbol{r}_q(t_e)) - \frac{\bar{R}(\boldsymbol{r}', \boldsymbol{r}_q(t_e))}{c\alpha^2} = 0. \tag{16}$$

Then, it can be shown that

$$Q(\boldsymbol{r}', t') = \frac{q(t_e)}{4\pi c^2 \bar{R}(\boldsymbol{r}', \boldsymbol{r}_q(t_e)) |\frac{dg}{dt}(t_e)|}. \tag{17}$$

Here, t_e is the emission time from the source point $\boldsymbol{r}_q$ for the signal received at observer location $\boldsymbol{r}'$ and observer time t'. We note that, for a stationary source point, t_e is the same as the retarded time t'_R defined in Eq. (11).

For convenience of discussion, define

$$\boldsymbol{R}_e = \boldsymbol{r}' - \boldsymbol{r}_q(t_e), \quad \boldsymbol{M}_e = \frac{1}{c}\frac{d\boldsymbol{r}_q}{dt}(t_e), \quad R_e = |\boldsymbol{R}_e|, \quad \text{and} \quad \bar{R}_e = \bar{R}(\boldsymbol{r}', \boldsymbol{r}_q(t_e)) = \sqrt{(\boldsymbol{M} \cdot \boldsymbol{R}_e)^2 + \alpha^2 R_e^2}. \tag{18}$$

Then, we have

$$\frac{d\bar{R}(\boldsymbol{r}', \boldsymbol{r}_q(t_e))}{dt} = -\frac{c\alpha^2}{\bar{R}_e} \left[(\boldsymbol{M} \cdot \boldsymbol{R}_e)(\boldsymbol{M} \cdot \boldsymbol{M}_e)/\alpha^2 + \boldsymbol{R}_e \cdot \boldsymbol{M}_e \right]$$

and

$$\frac{dg(t_e)}{dt} = -1 - c\boldsymbol{\beta} \cdot \boldsymbol{M}_e - \frac{1}{c\alpha^2}\frac{d\bar{R}(\boldsymbol{r}', \boldsymbol{r}_q(t_e))}{dt}$$

$$= -1 - (\boldsymbol{M} \cdot \boldsymbol{M}_e)/\alpha^2 + \frac{1}{\bar{R}_e}\left[(\boldsymbol{M} \cdot \boldsymbol{R}_e)(\boldsymbol{M} \cdot \boldsymbol{M}_e)/\alpha^2 + \boldsymbol{R}_e \cdot \boldsymbol{M}_e \right].$$

Upon simplification, we get the following expression for computing the contribution by a moving source at an observer point $\boldsymbol{r}'$ and observer time t':

$$Q(\boldsymbol{r}', t') = \frac{q(t_e)}{4\pi c^2 \left(\bar{R}_e - \boldsymbol{M}_e \cdot \boldsymbol{R}_e + \left(\boldsymbol{M} \cdot \boldsymbol{M}_e/\alpha^2\right)\left(\bar{R}_e - \boldsymbol{M} \cdot \boldsymbol{R}_e\right)\right)} \tag{19}$$

As a special case, in the absence of a mean flow, i.e., $\boldsymbol{M} = 0$, we get

$$Q(\boldsymbol{r}', t') = \frac{q(t_e)}{4\pi c^2 \left(R_e - \boldsymbol{R}_e \cdot \boldsymbol{M}_e\right)}, \tag{20}$$

which is the familiar expression for moving sources in a static medium (see, e.g., [10, 12, 13]).

III. Non-uniform Grid Interpolation Distribution Algorithm

The TDBIE, given by Eq. (12), will be solved using the Time Domain Boundary Element Method (TDBEM), which leads to a March-On-in-Time (MOT) scheme. Further details of the TDBEM can be found in Ref. [8], where a Burton-Miller reformulation of the TDBIE is employed for stabilization. We note that implementation of the Burton-Miller reformulation requires taking spatial and temporal derivatives of Eq. (12), as was done in Ref. [8] for the case of stationary sources. These derivatives are straightforward to carry out and will not be included in the present paper.

In a time-marching scheme, Eq. (10) or Eq. (12), including the source contribution term $Q(\boldsymbol{r}', t')$, must be evaluated on a uniformly spaced time grid $t'_n = n\Delta t$, referred to as the *observer time grid*. To compute $Q(\boldsymbol{r}', t'_n)$ using Eq. (19), however, the emission time t_e for the observer time must be determined using Eq. (16), which is an implicit equation for a moving source point. Finding t_e can be computationally expensive, especially when it must be determined for every observer point at each time step. In scattering problems, this becomes particularly demanding because every surface element on the scattering body serves as an observer.

Alternatively, computing the advanced time t' for a given emission time t_e is explicit. Let $t_j = j\Delta t$, where j is an integer, denote the emission time on the source time grid, and let t_j^{adv} represent the advanced time, or the arrival time, at an observer point $\boldsymbol{r}'$ for the signal emitted at t_j from a source point located at $\boldsymbol{r}_q(t_j)$. Then, t_j^{adv} can be computed explicitly:

$$t_j^{adv} = t_j - \boldsymbol{\beta} \cdot (\boldsymbol{r}' - \boldsymbol{r}_q(t_j)) + \frac{\bar{R}(\boldsymbol{r}', \boldsymbol{r}_q(t_j))}{c\alpha^2}. \tag{21}$$

The sequence of t_j^{adv} will be referred to as the *advanced time grid* corresponding to the *source time grid* t_j.

Although the source time grid t_j is uniformly spaced, its corresponding advanced time grid t_j^{adv} becomes non-uniform when the source is in motion. Interpolation is typically required to evaluate the acoustic field at a desired uniformly spaced observer time grid t'_n. In the following, we describe an efficient and accurate method for computing $Q(\boldsymbol{r}', t'_n)$ on the observer time grid t'_n.

For brevity, denote

$$u(t') \equiv Q(\boldsymbol{r}', t') \tag{22}$$

$$u_j^{adv} \equiv u(t_j^{adv}) = Q(\boldsymbol{r}', t_j^{adv}). \tag{23}$$

That is, u_j^{adv} denotes the value of the source contribution term received at the observer point $\boldsymbol{r}'$ at time t_j^{adv} due to the emission by source point $\boldsymbol{r}_q$ at source time t_j. In general, t_j^{adv} will not coincide with the observer time grid t'_n used in the computation of TDBEM. Let $t_{j-1}^{adv} < t'_n \le t_j^{adv}$ and suppose we use the following interpolation scheme:

$$u(t'_n) = \sum_{\ell=-K}^{N} u_{j+\ell}^{adv} L_j^{\ell}(t'_n) = u_{j-K}^{adv} L_j^{-K}(t'_n) + \cdots + u_j^{adv} L_j^{0}(t'_n) + \cdots + u_{j+N}^{adv} L_j^{N}(t'_n) \tag{24}$$

where $u_{j+\ell}^{adv}$ is the value received at the same observer due to the emission by the source point at source time $t_{j+\ell}$, and $L_j^{\ell}(t')$ stands for the Lagrange interpolation polynomials defined as:

$$L_j^{\ell}(t') = \frac{\Pi_{k=-K, k\neq\ell}^{k=N} (t' - t_{j+k}^{adv})}{\Pi_{k=-K, k\neq\ell}^{N} (t_{j+\ell}^{adv} - t_{j+k}^{adv})}. \tag{25}$$

The interpolation scheme uses K points to the left (past) and N points to the right (future) of t_j^{adv} on the advanced time axis, as illustrated in Fig. 1. To perform the interpolation directly, the acoustic values u_{j-K}^{adv} through u_{j+N}^{adv}, in addition to u_j^{adv}, must be computed or stored. This requirement may lead to repeated computations or increased storage demands. The interpolation scheme, Eq. (24), however, can be converted into a distribution scheme where no repeated computation of acoustic values is necessary. Define the following basis function $\psi_j(t')$ for a nodal point t_j^{adv}:

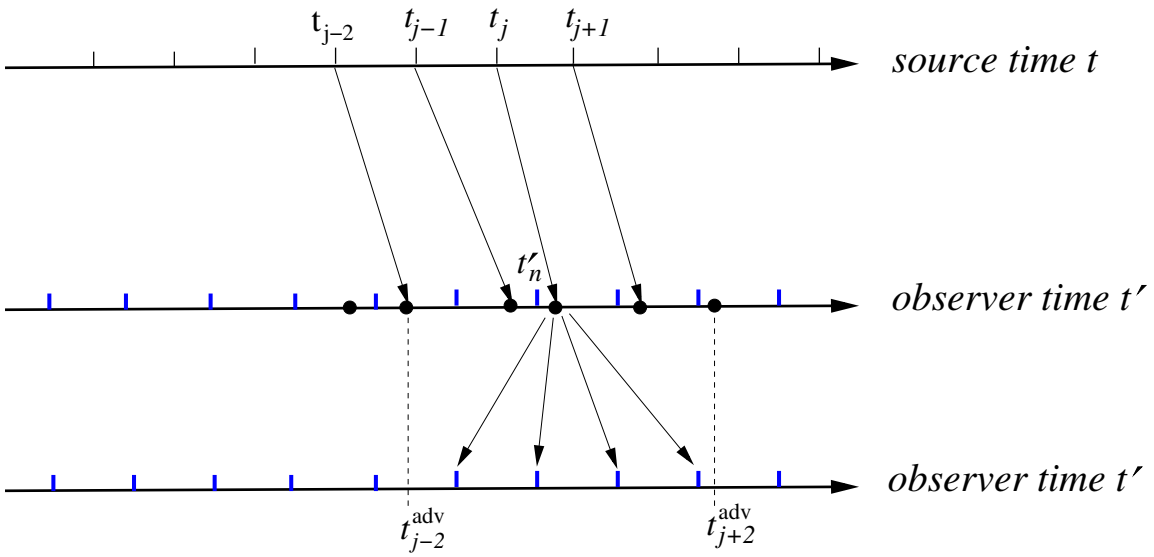

Figure 1 An illustration of NGIDA for the case of $K = 2$ and $N = 1$. While the value of acoustic field at a uniformly spaced observer grid point t'_n can be found by an interpolation using the values at t^{adv}_{j-2} to t^{adv}_{j+1}, the same interpolation can also be converted into a distribution of value u^{adv}_j to each t'_n that satisfies $t^{adv}_{j-2} < t'_n \le t^{adv}_{j+2}$ as illustrated.

$$\psi_j(t') = \begin{cases} L^N_{j-N}(t') & t^{adv}_{j-N-1} < t' \le t^{adv}_{j-N} \\ \vdots & \\ L^1_{j-1}(t') & t^{adv}_{j-2} < t' \le t^{adv}_{j-1} \\ L^0_j(t') & t^{adv}_{j-1} < t' \le t^{adv}_{j} \\ L^{-1}_{j+1}(t') & t^{adv}_{j} < t' \le t^{adv}_{j+1} \\ \vdots & \\ L^{-K}_{j+K}(t') & t^{adv}_{j+K-1} < t' \le t^{adv}_{j+K} \\ 0 & other \end{cases} \tag{26}$$

Then, the interpolation scheme shown in Eq. (24) can be equivalently written as

$$u(t'_n) = \sum_{\ell=-K}^{N} u^{adv}_{j+\ell}\psi_{j+\ell}(t'_n) = u^{adv}_{j-K}\psi_{j-K}(t'_n) + \cdots + u^{adv}_j\psi_j(t'_n) + \cdots + u^{adv}_{j+N}\psi_{j+N}(t'_n) \tag{27}$$

We note that the interpolation scheme for $u(t'_n)$, Eq. (27), where $t^{adv}_{j-1} < t'_n \le t^{adv}_j$, is a sum of contributions from u^{adv}_{j-K} to u^{adv}_{j+N}. ***Therefore, each acoustic value u^{adv}_j contributes a partial sum to $u(t'_n)$ for those t'_n on the uniformly spaced observer time grid that satisfy $t^{adv}_{j-N-1} < t'_n \le t^{adv}_{j+K}$, with the contribution equal to $u^{adv}_j\psi_j(t'_n)$.*** Based on this observation, we can construct an algorithm in which, once u^{adv}_j is computed, it can be immediately distributed to the corresponding $u(t'_n)$ on the uniformly spaced observer time grid. By doing so, no storage or repeated calculation of acoustic values is required.

We note that, in order to compute $\psi_j(t')$ as defined by Eq. (26), the values of t^{adv}_{j-N-K} through t^{adv}_{j+N+K} are also required. These correspond to the advanced time values for the source time t_{j-N-K} to t_{j+N+K}.

Specifically, the computation proceeds as follows:

1. Given a current time step t_j, compute its advanced time t^{adv}_j as well as the advanced times t^{adv}_{j-N-K} through t^{adv}_{j+N+K} corresponding to emission times t_{j-N-K} to t_{j+N+K}, using Eq. (21);

2. Determine all observer time grid points $t'_{n_i} = n_i \Delta t$ that satisfy the condition $t^{adv}_{j-N-1} < t'_{n_i} \le t^{adv}_{j+K}$, $i = 1, 2, ..., s$, where $n_1 = \text{ceiling}\left(t^{adv}_{j-N-1}/\Delta t\right)$, $n_s = \text{floor}\left(t^{adv}_{j+K}/\Delta t\right)$, and $s = n_s - n_1 + 1$;

3. Compute $\psi_j(t'_{n_i})$ for each t'_{n_i}, $i = 1, 2, ..., s$, using Eq. (26);

4. Compute u^{adv}_j and add $u^{adv}_j \psi_j(t'_{n_i})$ to $u(t'_{n_i})$, for $i = 1, 2, ..., s$.

This algorithm will be referred to as the Non-uniform Grid Interpolation Distribution Algorithm (NGIDA).

As an example, suppose we use the 3rd-order Lagrange interpolation polynomials with $K = 2$, $N = 1$. The NGIDA approach for computing the distribution of u^{adv}_j to each relevant $u(t'_n)$ on the observer time grid is as follows:

1. Given a current time step t_j, compute advance time t^{adv}_{j-3}, t^{adv}_{j-2}, t^{adv}_{j-1}, t^{adv}_j, t^{adv}_{j+1}, t^{adv}_{j+2}, t^{adv}_{j+2}, and t^{adv}_{j+3}, using Eq. (21), i.e., $t^{adv}_{j+\ell} = t_{j+\ell} - \boldsymbol{\beta} \cdot (\boldsymbol{r}' - \boldsymbol{r}_q(t_{j+\ell})) + \bar{R}(\boldsymbol{r}', \boldsymbol{r}_q(t_{j+\ell}))/c\alpha^2$, for $\ell = -3$ to 3;

2. Determine all uniformly spaced observer time grid points $t'_{n_i} = n_i \Delta t$ that satisfy $t^{adv}_{j-2} < t'_{n_i} < t^{adv}_{j+2}$, $i = 1, 2, ..., s$, where $n_1 = \text{ceiling}\left(t^{adv}_{j-N-1}/\Delta t\right)$, $n_s = \text{floor}\left(t^{adv}_{j+K}/\Delta t\right)$, and $s = n_s - n_1 + 1$;

3. Compute $\psi_j(t'_{n_i})$ for each t'_{n_i}, $i = 1, 2, ..., s$, where

$$\psi_j(t') = \begin{cases} L^1_{j-1}(t') = \dfrac{\left(t'-t^{adv}_{j-3}\right)\left(t'-t^{adv}_{j-2}\right)\left(t'-t^{adv}_{j-1}\right)}{\left(t^{adv}_j-t^{adv}_{j-3}\right)\left(t^{adv}_j-t^{adv}_{j-2}\right)\left(t^{adv}_j-t^{adv}_{j-1}\right)} & t^{adv}_{j-2} < t' \le t^{adv}_{j-1} \\ L^0_j(t') = \dfrac{\left(t'-t^{adv}_{j-2}\right)\left(t'-t^{adv}_{j-1}\right)\left(t'-t^{adv}_{j+1}\right)}{\left(t^{adv}_j-t^{adv}_{j-2}\right)\left(t^{adv}_j-t^{adv}_{j-1}\right)\left(t^{adv}_j-t^{adv}_{j+1}\right)} & t^{adv}_{j-1} < t' \le t^{adv}_j \\ L^{-1}_{j+1}(t') = \dfrac{\left(t'-t^{adv}_{j-1}\right)\left(t'-t^{adv}_{j+1}\right)\left(t'-t^{adv}_{j+2}\right)}{\left(t^{adv}_j-t^{adv}_{j-1}\right)\left(t^{adv}_j-t^{adv}_{j+1}\right)\left(t^{adv}_j-t^{adv}_{j+2}\right)} & t^{adv}_j < t' \le t^{adv}_{j+1} \\ L^{-2}_{j+2}(t') = \dfrac{\left(t'-t^{adv}_{j+1}\right)\left(t'-t^{adv}_{j+2}\right)\left(t'-t^{adv}_{j+3}\right)}{\left(t^{adv}_j-t^{adv}_{j+1}\right)\left(t^{adv}_j-t^{adv}_{j+2}\right)\left(t^{adv}_j-t^{adv}_{j+3}\right)} & t^{adv}_{j+1} < t' \le t^{adv}_{j+2} \\ 0 & other \end{cases}$$

4. Compute u^{adv}_j and add $u^{adv}_j \psi_j(t'_{n_i})$ to $u(t'_{n_i})$, for $i = 1, 2, ..., s$

Figure 2 shows examples of the basis function $\psi_j(t')$ for the cases of (a) $K = 1$, $N = 0$, 1st-order, (b) $K = 2$, $N = 0$, 2rd-order, (c) $K = 2$, $N = 1$, 3rd-order, and (d) $K = 3$, $N = 1$, 4th-order. As an illustration, a non-uniform grid of t^{adv}_j is assumed and indicated in closed circles in the figures. A value of acoustic signal u^{adv}_j contributes an amount $u^{adv}_j \psi(t')$ as a partial sum to the value of $u(t')$ where $t^{adv}_{j-N-1} < t' \le t_{j+K}$.

We also note that, since the advanced time grid t^{adv}_j is non-uniform for moving sources, the basis function $\psi_j(t')$ associated with each time node t^{adv}_j varies from node to node and depends on neighboring nodes from t^{adv}_{j-N-K} to t^{adv}_{j+N+K}. For this reason, the sequence of advanced time grid from t^{adv}_{j-N-K} to t^{adv}_{j+N+K} needs to be computed simultaneously with t^{adv}_j. It is expected that computation of t^{adv}_{j-N-K} to t^{adv}_{j+N+K}, which requires only the motion of the source, is much less costly compared to the computation of the acoustic signal u^{adv}_{j-K} to u^{adv}_{j+N} when the interpolation scheme, Eq. (24), is carried out directly. The NGIDA method is also applicable to stationary sources, for which the advanced time grid is uniformly spaced, as was done in Ref. [14]. For stationary sources, we simply have $t^{adv}_{j+\ell} = t^{adv}_j + \ell \Delta t$.

The NGIDA method described above pertains to propagation from a single source. When multiple sources are involved, such as integration over a source surface or a source region, contributions from all sources are to be aggregated on the uniformly spaced observer grid where the contribution from each source follows the NGIDA method.

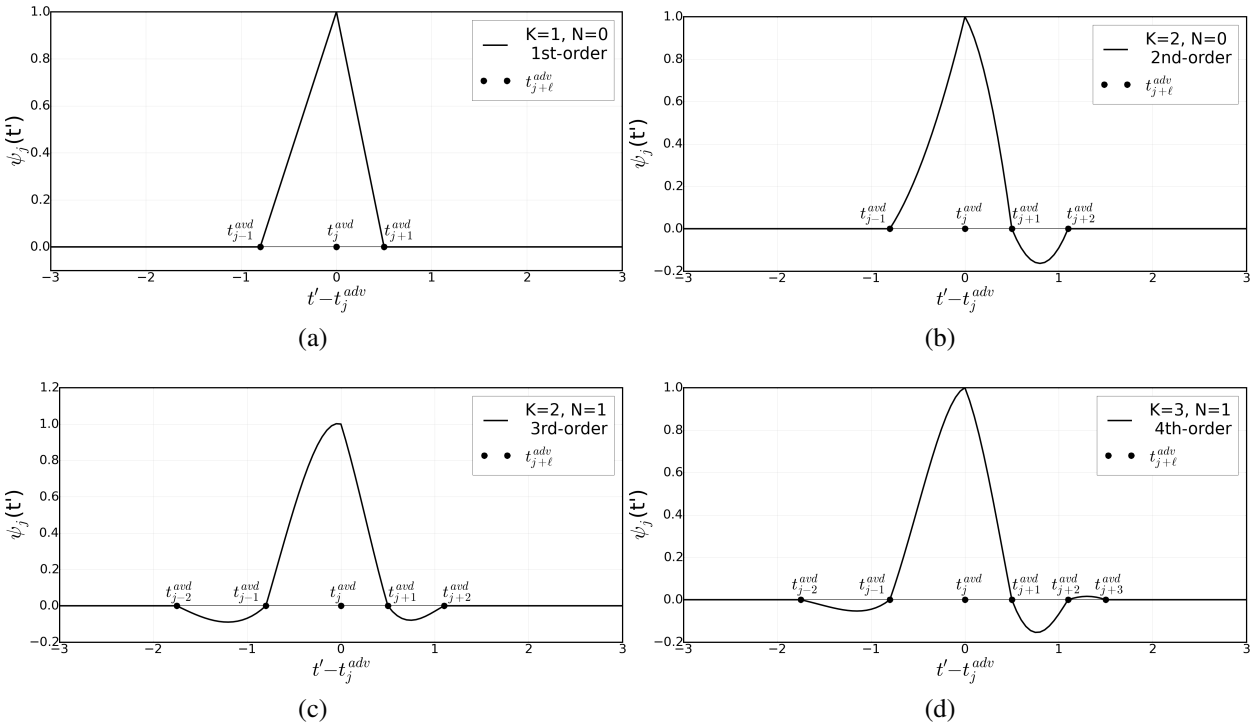

Figure 2 Examples of basis function $\psi_j(t')$ as defined by Eq. (26), for cases of (a) $K = 1$, $N = 0$, 1st-order, (b) $K = 2$, $N = 0$, 2nd-order, (c) $K = 2$, $N = 1$, 3rd-order, and (d) $K = 3$, $N = 1$, 4th-order. The non-uniform advanced time grid is shown in closed circles.

IV. Numerical examples

This section presents numerical examples of acoustic wave scattering by moving sources. The examples are selected to permit direct comparison with known analytical solutions, for validation of the mathematical formulation and its computational implementation. For computational results reported in this paper, the basis function of $K = 3$ and $N = 1$ by the 4th-order Lagrange polynomials is used in the NGIDA method.

A. Rotational sources

A numerical example is presented for the scattering of a rotating point source by a flat plate. In non-dimensional units, the plate is formed by a solid body with dimension $(x/L, y/L, z/L) \in [-2, 2] \times [-2, 2] \times [-0.1, 0]$, where L denotes the length scale for non-dimensionalization. A rotating point source is located above the top surface of the plate, as illustrated in Fig. 3. The point source is rotating as well as emitting acoustic waves.

The rotational motion of the point source is given by

$$\boldsymbol{r}_q(t) = \boldsymbol{r}_0 + (a_0 \cos(\omega_0 t), 0, a_0 \sin(\omega_0 t)) \tag{28}$$

where the center of rotation is at $\boldsymbol{r}_0 = (0, 0, 0.5L)$ and the radius and angular frequency of rotation are respectively $a_0/L = 0.25$ and $\omega_0 L/c = \pi/2$. The source term, as appearing in Eq. (1), is given by

$$s(\boldsymbol{r}, t) = \sin(\omega_s t)\delta\left(\boldsymbol{r} - \boldsymbol{r}_q(t)\right) \tag{29}$$

where ω_s is the frequency of the acoustic wave emitted by the rotating point source. A uniform mean flow of Mach number $M = 0.25$ in the direction of x-axis is assumed for the example.

A solid surface boundary condition is applied on the surface of the plate. That is, we assume[8]

$$\frac{\partial p}{\partial \tilde{n}} = 0 \quad \text{on the surface of plate.} \tag{30}$$

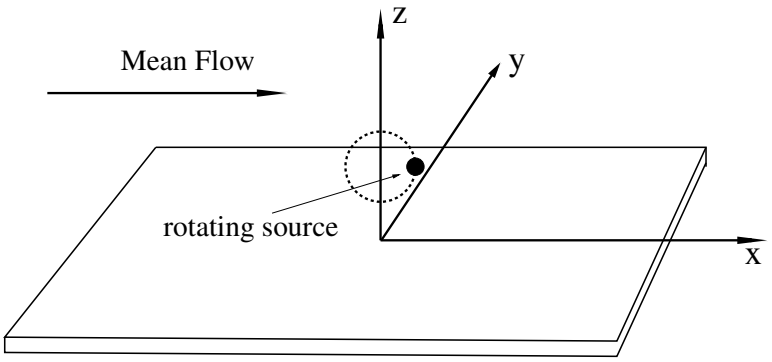

Figure 3 Schematic of a rotating point source above a flat plate.

The TDBIE, Eq. (12), is solved numerically by a Time Domain Boundary Element Method (TDBEM). Details on the numerical method can be found in Ref.[8]. The surface of the plate is discretized using a total of 88,000 rectangular elements.

Figure 4 shows four instantaneous contour plots of the numerical solution within one complete period of rotation. The source frequency is $\omega_s L/c = 4\pi$. Reflection of the acoustic wave by the plate and effects of rotation and mean flow are evident. As a validation of the mathematical formulation and computational implementation, Fig. 5 shows a comparison of the numerical solution with that of a reference solution. The reference solution is generated by placing a mirror image of the rotating point source with respect to the top surface of the plate in a domain free of the solid body. Specifically, the image source is

$$\boldsymbol{r}_q^{image}(t) = \boldsymbol{r}_0^{image} + (a_0\cos(\omega_0 t), 0, -a_0\sin(\omega_0 t)) \tag{31}$$

where $\boldsymbol{r}_0^{image} = (0, 0, -0.5L)$. Numerical and reference solutions at two selected locations as functions of time over two complete period of rotation are plotted in Fig. 5. The top figure is for a location upstream of the point source and the bottom figure is for a location downstream of the point source. Excellent agreement between the numerical and reference solutions is observed for both sample locations. The Doppler effect due to the rotational motion of the source point, as well as the mean flow effects, are clearly evident.

B. Sources in rectilinear motion

In this example, we consider the scattering of an acoustic field generated by a point source in rectilinear motion. The scattering surface is a flat plate, as in the previous example. Both solid and lined surface conditions will be studied. This example is selected because it can be compared with the scenario of a stationary point source in a uniform mean flow, for which an analytical solution is available for an infinitely large flat surface.

Figure 6 shows the schematic of a point source moving above a flat plate. The plate is of dimension $(x/L, y/L, z/L) \in [-4, 4] \times [-4, 4] \times [-0.1, 0]$. Here, L again denotes the length scale for non-dimensionalization. A point source is moving parallel to the surface of the plate in the direction of the x-axis in a trajectory defined by

$$\boldsymbol{r}_q(t) = (x_s + U_s t, y_s, z_s) \tag{32}$$

in which the initial position of the source point at time $t = 0$ is at $x_s/L = -3.0$, $y_s = 0$, and $z_s/L = 0.5$, and U_s denotes the velocity of the motion. The source point is emitting acoustic wave of frequency ω_s as it moves, with a source term as given in Eq. (29). The Mach number of the source motion is 0.25, and the source frequency is $\omega_s L/c = 4\pi$.

1. Solid surface

The numerical results for the case of a solid surface are presented first. Figure 7 shows instantaneous contour plots of the solution generated by the point source, along with its reflection from the surface of the plate, as the source moves parallel to the surface. The time history of acoustic pressure at an observer located at $\boldsymbol{r}_0 = (x_0, y_0, z_0)$ is shown in Fig. 8, with $x_0 = y_0 = 0$ and $z_0/L = 0.25$. The maximum occurs at a time t_0 when the source point is directly above

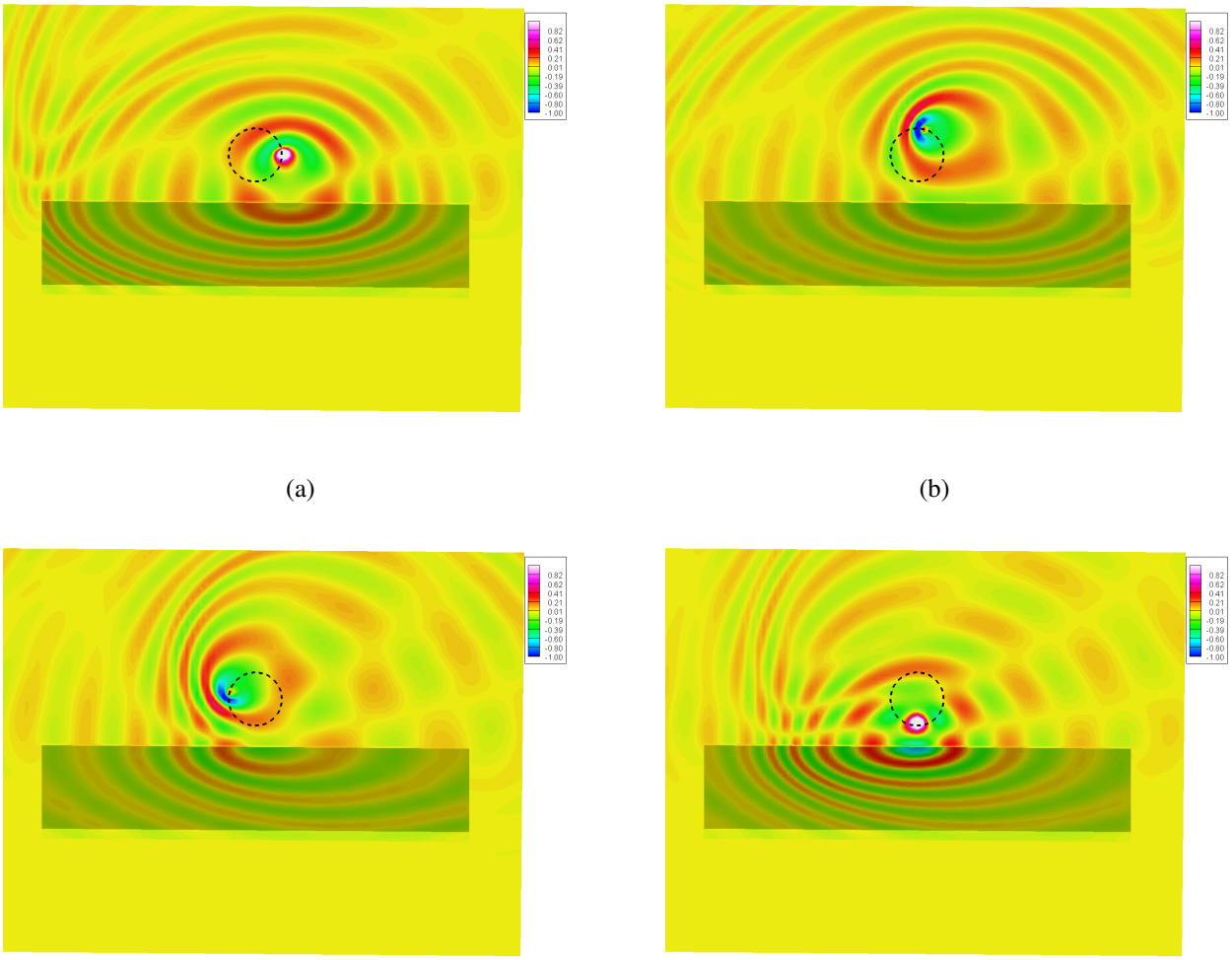

Figure 4 Snapshots of contours of scattered field over one rotation cycle. Sub-plots (a)-(d) span a full period of rotation. The dashed line indicates the rotational trajectory of the source. The contour levels represent SPL non-dimensionalized by $\rho_0 c^2$ where ρ_0 is the mean density of fluid.

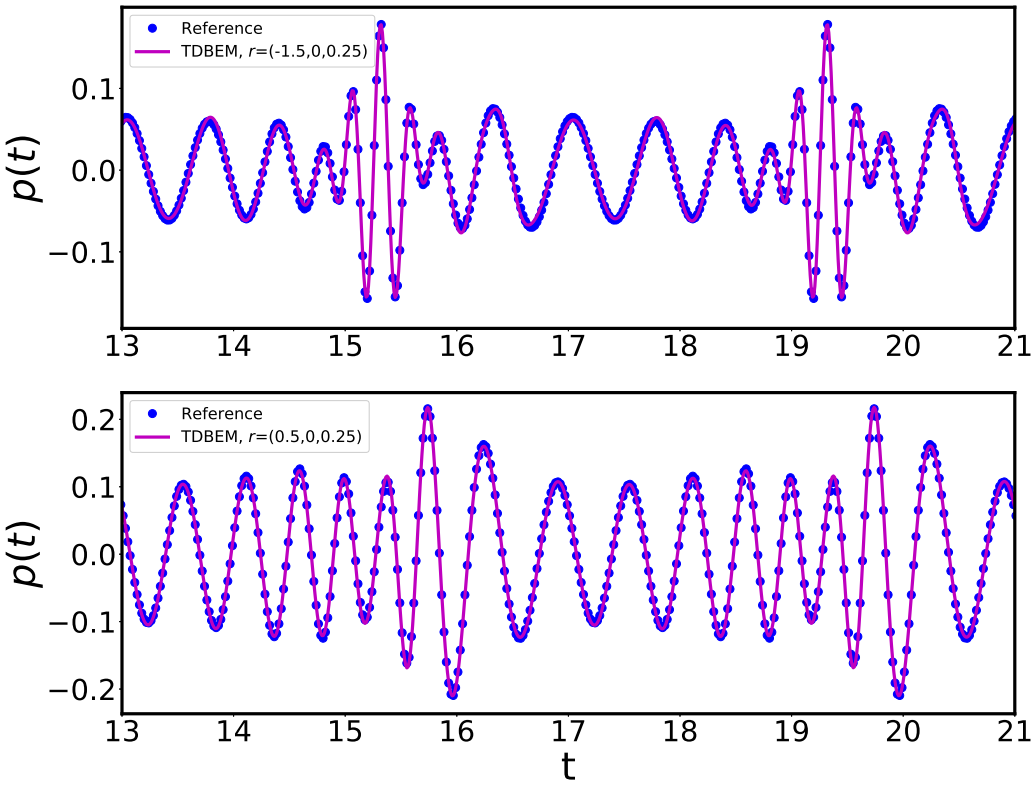

Figure 5 Time history of numerical solution (solid lines) at two selected locations and comparison with the reference solution (symbols). The time shown is non-dimensionalized by L/c.

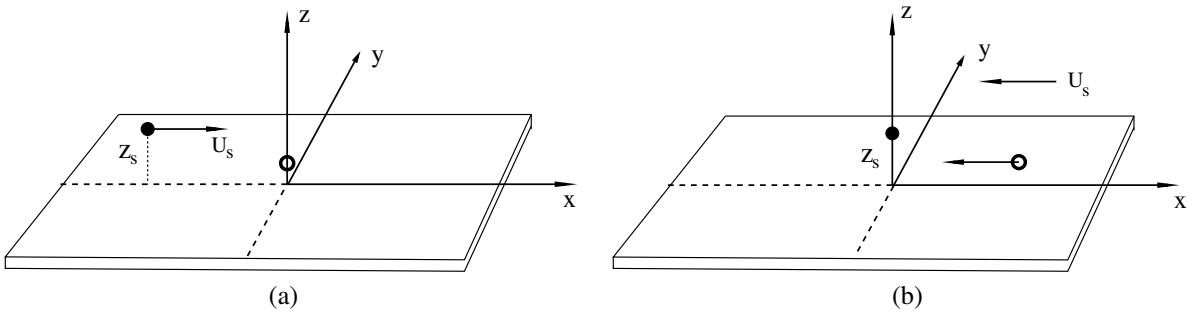

Figure 6 Schematic of a point source moving above a flat plate. (a) Point source moving with a velocity U_s in a static medium; (b) Point source is stationary in a mean flow of velocity $-U_s$. • source point; ∘ observer point.

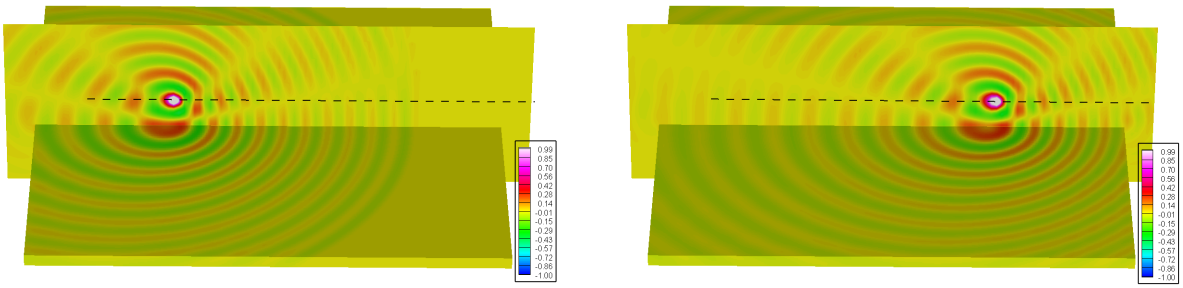

(a) (b)

Figure 7 Snapshots of contours of a moving point source above a plate of solid surfaces. The dashed line indicates the trajectory of motion. (a) $ct/L = 6$;**(b)** $ct/L = 19$**. The contour levels represent SPL non-dimensionalized by** $\rho_0 c^2$ **where** ρ_0 **is the mean density of fluid.**

the observer point. The Doppler effect due to the motion of the source is evident, as Fig. 8, shows that the observed frequency is higher for $t < t_0$, when the source point is approaching the observer point, than for $t > t_0$, when the source is moving away.

A comparison with the analytical solution is also provided in Fig. 8. The analytical solution corresponds to an equivalent scenario in which the source is stationary but a mean flow is imposed in the direction opposite to the source's original direction of motion, as illustrated in Fig. 6. A detailed derivation of the analytical solution is presented in the Appendix. Excellent agreement between the numerical and analytical results is observed.

2. Lined surface

The situation of an acoustically lined flat plate (top surface) is now considered. The liner impedance condition, in a static medium, is given by

$$\frac{\hat{p}(\boldsymbol{r}_s, \omega)}{\hat{u}_{\mathrm{n}}(\boldsymbol{r}_s, \omega)} = Z(\omega), \tag{33}$$

where $\hat{p}$ is the pressure of the acoustic wave and $\hat{u}_{\mathrm{n}}$ is the velocity component normal to the liner surface, pointing outward from the domain. Here, $\boldsymbol{r}_s$ is the position vector on the liner surface, $Z(\omega)$ denotes the liner impedance at frequency ω, and a caret has been used to denote variables in the frequency domain.

By the Euler equations for inviscid fluids, we have the following relation between u_n and the normal acoustic pressure derivative $\partial p/\partial n$ when no mean flow is present:

$$\frac{\partial u_n}{\partial t} + \frac{1}{\rho_0}\frac{\partial p}{\partial n} = 0, \tag{34}$$

where ρ_0 is the mean density of the fluid. Then, the impedance condition (Eq. 33) can also be expressed as

$$\rho_0 \, (i\omega) \, \hat{p}(\boldsymbol{r}_s, \omega) = Z(\omega) \frac{\partial \hat{p}}{\partial n}(\boldsymbol{r}_s, \omega). \tag{35}$$

In the present paper, the impedance function $Z(\omega)$ is modeled by a multipole expression as[15, 16]

$$Z(\omega) = -i\omega h_0 + R_0 + \sum_{m=1}^{N_0} \frac{A_m}{\lambda_m - i\omega} + \frac{1}{2}\sum_{\ell=1}^{L_0}\left[\frac{B_\ell + iC_\ell}{\alpha_\ell + i\beta_\ell - i\omega} + \frac{B_\ell - iC_\ell}{\alpha_\ell - i\beta_\ell - i\omega}\right]. \tag{36}$$

For the current example, the coefficients of the liner multipole model (with $N_0 = 1$ and $L_0 = 2$), normalized by $\rho_o c$, are as follows:

$$h_0 = 0.013885, \; R_0 = 0.293936, \; \lambda_1 = 0.116633, \; A_1 = 16.493641,$$

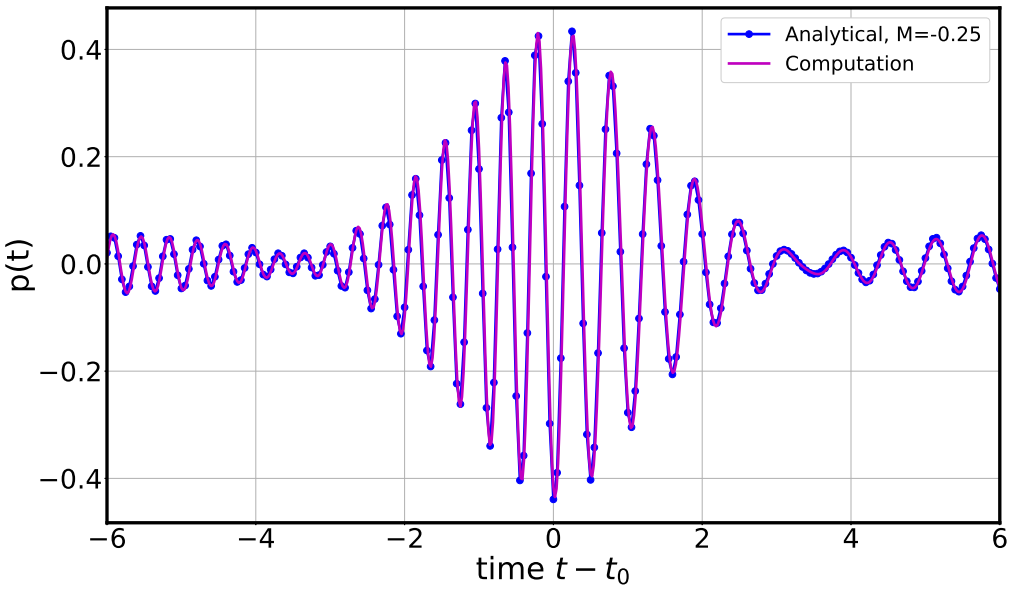

Figure 8 Time history of numerical solution at observer point $(0, 0, 0.25L)$, above a hardwall surface, and comparison with the analytical solution. The time shown is non-dimensionalized by L/c.

$$\alpha_1 = 4.109402,\ \beta_1 = 37.478310,\ B_1 = 12.089093,\ C_1 = -1.296148,$$
$$\alpha_2 = 3.861189,\ \beta_2 = 35.014072,\ B_2 = 23.308557,\ C_2 = -0.245725.$$

The resistance and reactance as functions of frequency are shown in Fig. 9.

Together with the multipole expression of the impedance by Eq. (36), the impedance boundary condition, Eq. (35), can be converted into a Time Domain Impedance Boundary Condition (TDIBC) as follows:

$$h_0 \frac{\partial p_n}{\partial t} + R_0 p_n = -\rho_0 \frac{\partial p}{\partial t} - \sum_{m=1}^{N_0} A_m p_m^{(0)} - \sum_{\ell=1}^{L_0} \left[B_\ell p_\ell^{(1)} + C_\ell p_\ell^{(2)} \right], \tag{37}$$

$$\frac{dp_m^{(0)}}{dt} + \lambda_m p_m^{(0)} = p_n, \quad m = 1, ..., N_0, \tag{38}$$

$$\frac{dp_\ell^{(1)}}{dt} + \alpha_\ell p_\ell^{(1)} + \beta_\ell p_\ell^{(2)} = p_n, \quad \frac{dp_\ell^{(2)}}{dt} + \alpha_\ell p_\ell^{(2)} - \beta_\ell p_\ell^{(1)} = 0, \quad \ell = 1, ..., L_0, \tag{39}$$

where p_n stands for the normal pressure derivative term $\partial p/\partial n$, and $p_m^{(0)}$, $m = 1, ..., N_0$, and $p_\ell^{(1)}$, $p_\ell^{(2)}$, $\ell = 1, ..., L_0$, are auxiliary variables that are introduced for the convenience of implementation.

Again, the TDBIE, (Eq. 12), coupled with the TDIBC, Eqs. (37)-(39), is solved by the TDBEM. Further details on the numerical method are provided in Ref. [17].

Figure 10 presents snapshots of instantaneous pressure contours as the acoustic source moves above a lined plate. The surface of the plate is a liner with the impedance boundary condition as defined in Eqs. (37)-(39). Due to the motion of the source, the frequency of the incident acoustic wave impinging on the surface varies with time as a result of the Doppler effect. Consequently, the impedance boundary is subjected to a range of frequencies, which is captured in the time-domain simulation through the time domain impedance boundary condition.

Figure 11 shows the comparison between numerical and analytical solutions. The analytical solution for the reflection of a moving point source by a lined surface is given in the appendix. Excellent agreement is observed, indicating the

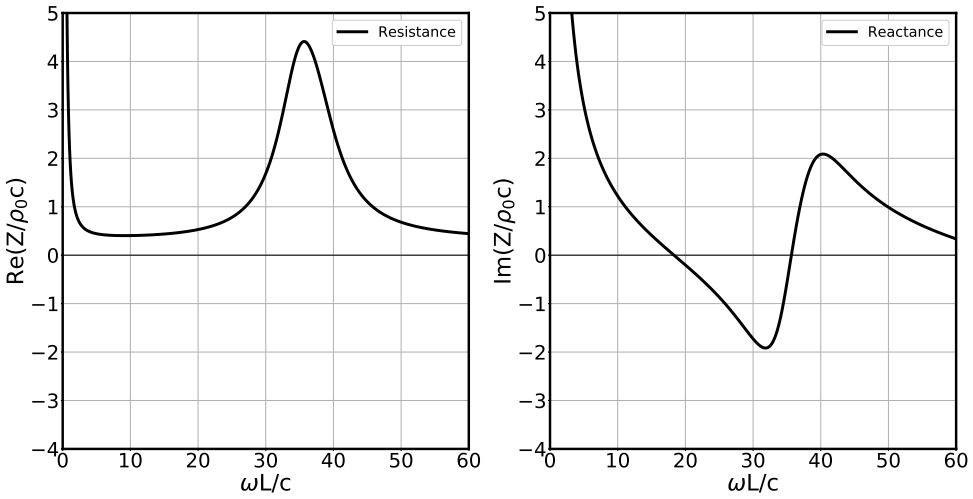

Figure 9 Impedance as a function of frequency, modeled by Eq. (36) and used in the numerical example in Sec. 4.B.

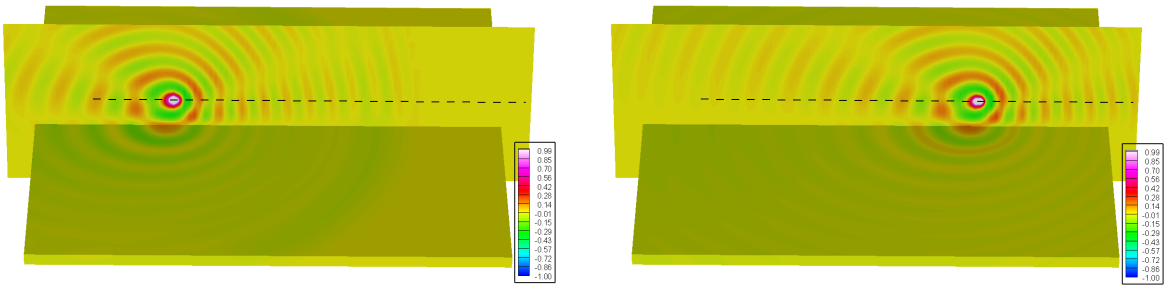

(a) (b)

Figure 10 A moving point source above a flat plate with a lined top surface. The dashed line indicates the trajectory of motion. (a) $ct/L = 6$;**(b)** $ct/L = 19$**.**

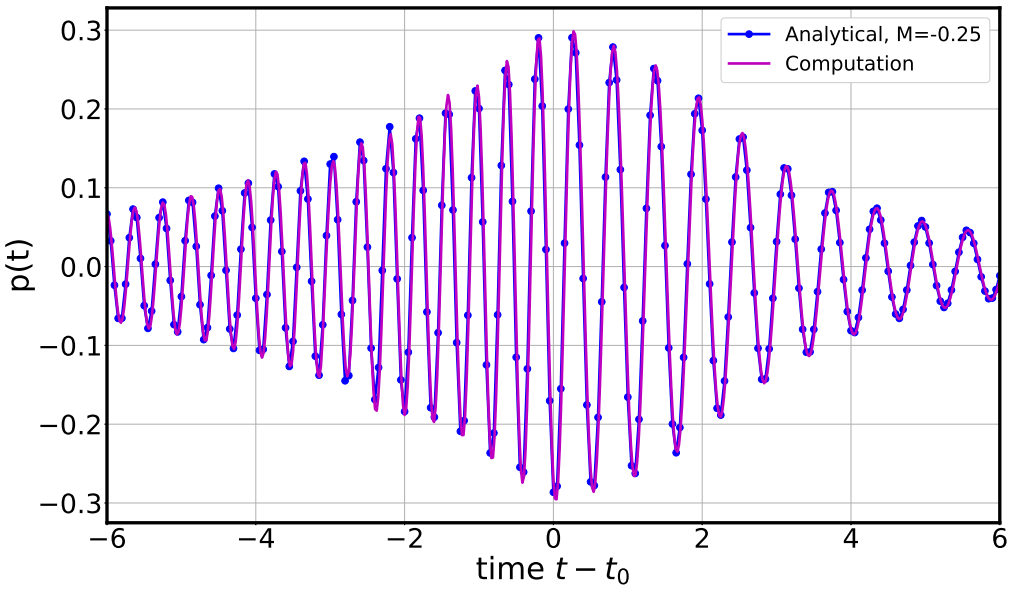

Figure 11 Time history of numerical solution at observer point located at $(0, 0, 0.25L)$, above a lined surface, and comparison with the analytical solution. The time shown is non-dimensionalized by L/c.

frequency-dependent behavior at the lined surface is accurately accounted for in the time domain simulation. We note that the analytical solution is derived for an infinitely large flat surface, while numerical simulation is performed with a flat plate of finite length. It appears, however, the diffraction effects by the plate edges are not significant for the solution at the chosen observer point which is located directly above the center of the plate.

V. Concluding remarks

A time-domain boundary integral equation for acoustic scattering has been formulated to include moving sources. While the solution procedure using the time-domain boundary element method follows a similar approach as for stationary sources, a key challenge arises from the fact that the sequence of observer times corresponding to a uniformly spaced source time sequence is no longer uniformly distributed. To avoid potentially costly root-finding procedures for computing retarded times, an advanced time propagation approach, called the Non-uniform Grid Integration Distribution Algorithm (NGIDA), has been proposed. This approach achieves high-order accuracy while avoiding repeated evaluations of the acoustic signal. The algorithm is also readily extendable to higher-order accuracy. Numerical examples of moving source scattering by a flat plate are presented, including both rotational and rectilinear moving sources. The plate surfaces considered include both rigid and acoustically treated configurations. Comparisons with analytical solutions demonstrate excellent agreement, validating both the mathematical formulation and numerical implementation. A limitation of the current formulation is that it is restricted to subsonic source motions. Improvements of NGIDA for sources with supersonic motions will be reported in future work.

Appendix

Analytical solution of a moving point source reflection by a lined surface

The analytical solutions of acoustic waves from a moving point source above an impedance plane has been studied in the literature (see, e.g. Ref. [18–20]). For completeness, we derive an analytical solution for a moving point source above an infinitely large flat surface with a general frequency-dependent impedance condition.

Consider the wave equation with a moving point source:

$$\frac{\partial^2 p}{\partial t^2} - c^2\nabla^2 p = q(t)\delta(x - x_s - U_s t)\delta(y - y_s)\delta(z - z_s) \tag{40}$$

We first apply a Galilean transformation from x to x_g:

$$x_g = x - U_s t. \tag{41}$$

Then we get

$$\left(\frac{\partial}{\partial t} - U_s\frac{\partial}{\partial x_g}\right)^2 p - c^2\nabla^2 p = q(t)\delta(x_g - x_s)\delta(y - y_s)\delta(z - z_s). \tag{42}$$

Define the Fourier transform

$$\hat{p}(\boldsymbol{r}_g, \omega) = \int_{-\infty}^{\infty} p(\boldsymbol{r}_g, t)e^{i\omega t}dt \tag{43}$$

and its inverse

$$p(\boldsymbol{r_g}, t) = \frac{1}{2\pi}\int_{-\infty}^{\infty} \hat{p}(\boldsymbol{r}_g, \omega)e^{-i\omega t}d\omega \tag{44}$$

where $\boldsymbol{r}_g \equiv (x_g, y, z)$.
We obtain the convective Helmholtz equation for $\hat{p}(\boldsymbol{r}_g, \omega)$:

$$\left(i\omega + U_s\frac{\partial}{\partial x_g}\right)^2 \hat{p} - c^2\nabla^2\hat{p} = \hat{q}(\omega)\delta(x_g - x_s)\delta(y - y_s)\delta(z - z_s). \tag{45}$$

The frequency domain solution to Eq. (45) in free space without any boundary is well-known [9]:

$$\hat{p}_{inc}(\boldsymbol{r}_g, \omega) = \hat{q}(\omega)e^{-iM\omega(x_g - x_s)/\alpha^2 c}\frac{e^{i\omega\bar{R}/\alpha c}}{4\pi\alpha c^2\bar{R}}, \tag{46}$$

where

$$\bar{R} = \sqrt{(x_g - x_s)^2/\alpha^2 + (y - y_s)^2 + (z - z_s)^2}, \quad \alpha = \sqrt{1 - M^2}. \tag{47}$$

and

$$M = -U_s/c.$$

It is straightforward to show that, similar to the Weyl identity for the regular wave equation with no flow, the incident point source, Eq. (46), can be expressed in plane waves as follows:

$$\hat{p}_{inc}(\boldsymbol{r}_g, \omega) = \frac{i\hat{q}(\omega)}{8\pi^2 c^2}\int_{-\infty}^{\infty}\int_{-\infty}^{\infty}\frac{1}{\gamma}e^{ik_x(x_g - x_s) + ik_y(y - y_s) + i\gamma|z - z_s|}dk_x dk_y, \tag{48}$$

where

$$\gamma = \sqrt{(\omega/c - Mk_x)^2 - \left(k_x^2 + k_y^2\right)}. \tag{49}$$

Only subsonic flows are considered, i.e., we assume $|M| < 1$. The branch-cut in the complex ω plane for the square-root function in Eq. (49) is such that

$$Im\left\{\sqrt{(\omega/c - Mk_x)^2 - \left(k_x^2 + k_y^2\right)}\right\} \geq 0. \tag{50}$$

Here, $Re\{\cdot\}$ and $Im\{\cdot\}$ denote respectively the real and imaginary parts of the expression inside the bracket.

Let the reflected wave be expressed as

$$\hat{p}_{ref}(\boldsymbol{r}_g,\omega)=\frac{i\hat{q}(\omega)}{8\pi^2c^2}\int_{-\infty}^{\infty}\int_{-\infty}^{\infty}\frac{R}{\gamma}e^{ik_x(x_g-x_s)+ik_y(y-y_s)+i\gamma(z+z_s)}dk_xdk_y \tag{51}$$

where R is the reflection coefficient. For the reflection by a solid surface, we have $R=1$. For a lined surface, R is determined by the impedance boundary condition.

Under the Galilean transformation (Eq. (41), the TDIBC (Eqs. (37)-(39), becomes

$$h_0\left(\frac{\partial p_n}{\partial t}-U_s\frac{\partial p_n}{\partial x_g}\right)+R_0p_n=-\rho_0\left(\frac{\partial p}{\partial t}-U_s\frac{\partial p}{\partial x_g}\right)-\sum_{m=1}^{N}A_mp_m^{(0)}-\sum_{\ell=1}^{L}\left[B_\ell p_\ell^{(1)}+C_\ell p_\ell^{(2)}\right], \tag{52}$$

$$\frac{dp_m^{(0)}}{dt}-U_s\frac{\partial p_m^{(0)}}{\partial x_g}+\lambda_m p_m^{(0)}=p_n,\quad m=1,...,N, \tag{53}$$

$$\frac{dp_\ell^{(1)}}{dt}-U_s\frac{\partial p_\ell^{(1)}}{\partial x_g}+\alpha_\ell p_\ell^{(1)}+\beta_\ell p_\ell^{(2)}=p_n,\quad \frac{dp_\ell^{(2)}}{dt}-U_s\frac{\partial p_\ell^{(2)}}{\partial x_g}+\alpha_\ell p_\ell^{(2)}-\beta_\ell p_\ell^{(1)}=0,\quad \ell=1,...,L, \tag{54}$$

It is straightforward to show that, for plane waves of wave number k_x, this leads to

$$\rho_0\hat{p}(\boldsymbol{r}_g,\omega)=Z(\omega+U_sk_x)\frac{\partial\hat{p}}{\partial n}(\boldsymbol{r}_g,\omega) \tag{55}$$

on the surface of the liner. That is, the impedance at a frequency of $\omega+U_sk_x$ should be applied for an incident plane wave with wave number k_x.

Then, the reflection coefficient is found to be the following

$$R=\frac{\gamma Z(\omega+U_sk_x)-\rho_0}{\gamma Z(\omega+U_sk_x)+\rho_0}. \tag{56}$$

Thus, the reflected wave is

$$\hat{p}_{ref}(\boldsymbol{r}_g,\omega)=\frac{i\hat{q}(\omega)}{8\pi^2c^2}\int_{-\infty}^{\infty}\int_{-\infty}^{\infty}\frac{1}{\gamma}\frac{\gamma Z(\omega+U_sk_x)-\rho_0}{\gamma Z(\omega+U_sk_x)+\rho_0}e^{ik_x(x_g-x_0)+ik_y(y-y_0)+i\gamma(z+z_0)}dk_xdk_y \tag{57}$$

and we have

$$p(\boldsymbol{r}_g,t')=\frac{1}{2\pi}\int_{-\infty}^{\infty}\left[\hat{p}_{in}(\boldsymbol{r}_g,\omega)+\hat{p}_{ref}(\boldsymbol{r}_g,\omega)\right]e^{-i\omega t}d\omega. \tag{58}$$

In the original physical coordinate, we have the solution for pressure as

$$p(x,y,z,t)=\frac{1}{2\pi}\int_{-\infty}^{\infty}\left[\hat{p}_{in}(x-U_st,y,z,\omega)+\hat{p}_{ref}(x-U_st,y,z,\omega)\right]e^{-i\omega t}d\omega. \tag{59}$$

The integrals appearing in Eq. (57) can be carried out in a similar way as in the case of stationary source above a lined surface. Further details may be found in Ref. [16, 21].

Acknowledgments

This research was funded by NASA's Advanced Air Transport Technology (AATT) Project and Revolutionary Vertical Lift Technology (RVLT) project. This work used the computational resources at the Old Dominion University ITS Turing cluster.

References

[1] Lyrintzis, A. S., and Xue, Y., "Toward a Versatile Kirchhoff's method code," *AIAA Journal*, Vol. 35, 1997, pp. 198–200.

[2] Ozyoruk, Y., and Long, L. N., "A new efficient algorithm for computational aeroacoustics on parallel computers," *Journal of Computational Physics*, Vol. 125, 1996, pp. 135–149.

[3] Casalino, D., "An advanced time approach for acoustic analogy predictions," *Journal of Sound and Vibration*, Vol. 261, 2003, pp. 583–612.

[4] Brentner, K. S., "Numerical algorithms for acoustic integrals – the devil is in the details," AIAA Paper 96-30821, 1996.

[5] Brentner, K. S., and Farassat, F., "Modeling aerodynamically generated sound of helicopter rotors," *Progress in Aerospace Sciences*, Vol. 39, 2003, pp. 83–120.

[6] Lopes, L. V., "ANOPP2's Farassat Formulations Integral Functional Modules (AFFIFMs) Reference Mannual," NASA-TM NASA-TM-20210021111, 2021.

[7] Hu, F. Q., "On hybrid temporal basis functions for stable numerical solution of time domain boundary integral equations," *Advances in Aerodynamics*, Vol. 1, 2019, p. article 9.

[8] Hu, F. Q., Pizzo, M. E., and Nark, D. M., "On a time domain boundary integral equation formulation for acoustic scattering by rigid bodies in uniform mean flow," *Journal of the Acoustical Society of America*, Vol. 142, 2017, pp. 3624–3636.

[9] Morse, P. M., and Ingard, K. U., *Theoretical Acoustics*, 1st ed., Princeton University Press, Princeton, NJ, 1986.

[10] Dowling, A. P., and Williams, J. E. F., *Sound and sources of sound*, 1st ed., Ellis Horwood Limitted, 1983.

[11] Crighton, D. G., Dowling, A. P., Williams, J. E. F., Heckl, M., and Leppington, F. G., *Modern Methods in Analytical Acoustics*, 1st ed., Springer-Verlag London Limmited, 1992.

[12] Farassat, F., "Linear acoustic formulas for calculation of rotating blade noise," *AIAA Journal*, Vol. 19, 1981, pp. 1122–1130.

[13] Farassat, F., and Myers, M. K., "Extension of Kirchhoff's formula to radiation from moving surfaces," *Journal of Sound and Vibration*, Vol. 123, 1988, pp. 451–460.

[14] Hu, F. Q., "An efficient solution of time domain boundary integral equations for acoustic scattering and its acceleration by Graphics Processing Units," AIAA Paper 2013-2018, 2013.

[15] Dragna, D., Pineau, P., and Blanc-Benon, P., "A Generalized Recursive Convolution Method for Time-Domain Propagation in Porous Media," *Journal of the Acoustical Society of America*, Vol. 138, 2015, pp. 1030–1042.

[16] Hu, F. Q., and Nark, D. M., "On a stabilization of the Ingard-Myers impedance boundary condition and its time domain implementation," *International Journal of Aeroacoustics*, Vol. 23, 2024, pp. 318–341.

[17] Rodio, M. E., Hu, F. Q., and Nark, D. M., "Time-Domain Boundary Element Method with Broadband Impedance Boundary Condition," *AIAA Journal*, Vol. 60, 2022, pp. 2661–3670.

[18] Norum, T. D., and Liu, C. H., "Point source moving above a finite impedance reflecting plane – experiment and theory," *Journal of Acoustical Society of America*, Vol. 63, 1978, pp. 1069–1073.

[19] Ochmann, M., "Exact solution for sound radiation from a moving monopole above an impedance plane," *Journal of Acoustical Society of America*, Vol. 133, 2013, pp. 1911–1921.

[20] Dragna, D., and Blanc-Benon, P., "Sound radiation by a moving line source above an impedance plane with frequency-dependent properties," *Journal of Sound and Vibration*, Vol. 349, 2015, pp. 259–275.

[21] Zheng, S., and Zhuang, M., "Three-dimensional benchmark problem for broadband time-domain impedance boundary conditions," *AIAA Journal*, Vol. 42, 2004, pp. 405–407.